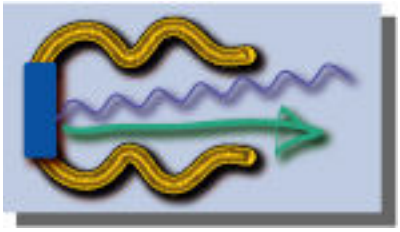

PHIN

Measurements of the Radio-Frequency Photo Electron Source with Superconducting Niobium Cavity (SRF Gun Measurement, Part 1)

J. Teichert, A. Arnold, H. Buettig , R. Hempel, D. Janssen, U. Lehnert, P. Michel, K. Moeller, P. Murcek, C. Schneider, R. Schurig, F. Staufenbiel, R. Xiang.

FZ Dresden-Rossendorf, Dresden, Germany,

Abstract

The report presents the measurements of the critical subsystems of the SRF photo injector carried out during the development phase of the photo injector. These measurements concern the niobium cavity, the cathode cooling system, the cavity tuners and some parts of the gun cryostat.

1. Introduction

During the last three years a superconducting rf photoelectron injector has been developed and built at the Forschungszentrum Dresden-Rossendorf (FZD) which will be installed at the superconducting linear accelerator ELBE. This work has been performed within a large national and international collaboration and with financial support of the European Commission and the German Federal Government.

The main components of the SRF photo-injector are shown in Fig. 1. The key element is the 3½ cell niobium cavity which is liquid He cooled. This cavity contains a normal-conducting photocathode with a caesium telluride photo-emission layer. Details of the injector design, expected electron beam parameters and status reports have been published in several papers [1-11].

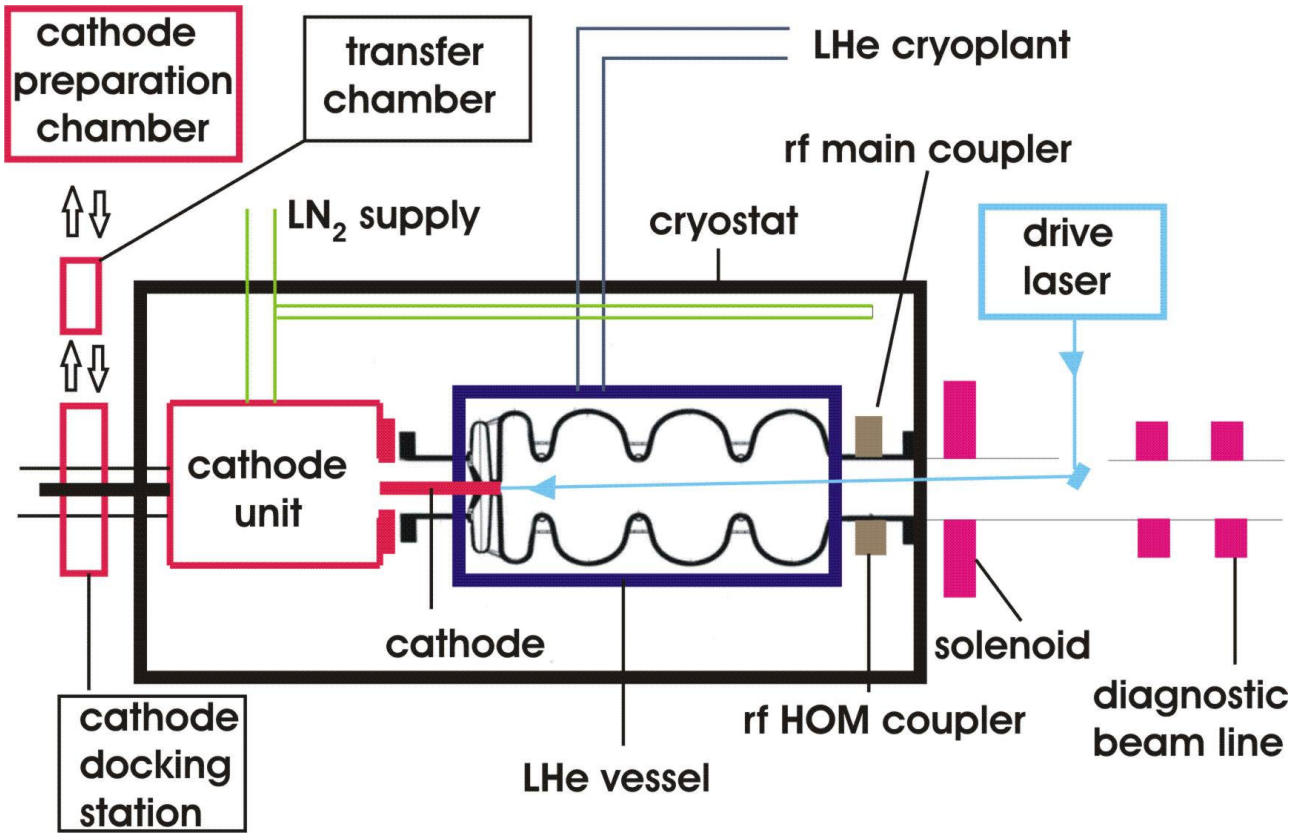

Fig.1. Basic layout of the SRF photo injector.

In comparison to superconducting accelerator modules the existence of a photocathode in the gun cell causes additional problems. In detail the following physical and technological problems are difficult to overcome:

1. The heat load introduced into the cavity by the presence of the photocathode may lead to break-down of superconductivity.
2. There are basically three sources which can cause heating of the cathode: heat conduction along the cathode stem, heating of the surface of the cathode by the photo

laser beam and heating by rf energy loss induced in the cathode by the cavity rf field, respectively.
3. The quality factor of the superconducting resonator may be deteriorated by impurities introduced by the cathode.
4. The long-term stability of the photocathode layer must be sufficient to allow for an effective operation of the gun.
5. The necessary focusing and emittance reduction by a solenoid cannot be performed close to the cathode where it is most efficient since the magnetic field of the solenoid would cause a break-down of superconductivity.
6. The special geometrical shape required for the gun cell may differ from a gun cell shape which is optimized only with respect to the maximum gradient condition.

As a consequence, several subsystems were developed and fabricated which differ essentially in their design from that of an accelerator module or a normal-conducting rf photo injector. The most critical subsystems are the niobium cavity with the choke filter, the photo cathode assembly with its cooling system, and the cavity tuners. For these components functional tests and parameter measurements were carried out. The present report describes these measurements of the subsystems. Later the second part will present the injector measurements after commissioning in summer 2007.

2. Photo Cathode Cooling System

The Rossendorf SRF gun uses a normal conducting photocathode which is inside the half-cell of the superconducting cavity. This has the advantage that a robust cathode like Cs_2Te with long life-time and high quantum efficiency can be applied. On the other side, the normal conducting cathode is a heat source in the cavity. There are three contributions: the power dissipation of the surface currents induced by the rf magnetic field, the dielectric losses caused by the rf electric field, and the power absorption in the photo cathode from the driver laser.

The photo cathode as shown in Fig. 2, has a cooper stem with a diameter of 10 mm. Since molybdenum is a preferred substrate material, the top part (about 1 cm long) consists of that material. On the front surface the Cs_2Te layer is deposited with a thickness between 10 to 50 nm. The rf magnetic field is zero on the axis and comparably low at the cathode surface. But the resistivity of the normal conducting cathode is about six orders of magnitude higher than that of the superconducting niobium. The typical skin depth of the rf field is 1 μm. The magnetic rf losses are mainly in the substrate. Therefore the power dissipation by the magnetic rf field can be exactly calculated with a code like SUPERFISH [12]. Results are shown in Table 1.

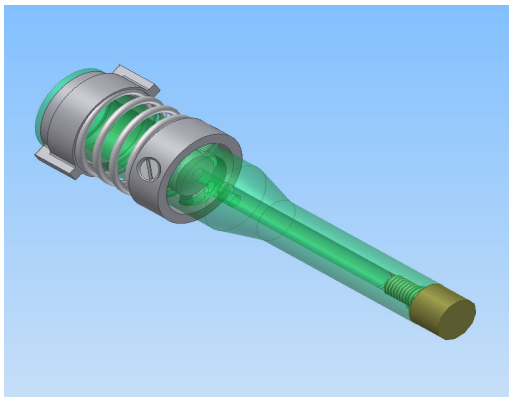

Fig. 2: Design of the SRF gun photocathode.

Table 1: Estimated power dissipation by the magnetic rf field in the photocathode obtained from SUPERFISH simulation.

cathode material	R_{surf}	P_{diss} @ 33 MV/m
Cu	9.4 mΩ	2.6 W
Mo	17.2 mΩ	4.6 W

It is rather difficult to calculate the dielectric losses in the Cs_2Te layer since the material parameters are unknown. A first estimation exists in ref. [13] which based on a measurement at 3 GHz [14]. For the present SRF gun the same estimation yields about 15 W.

The UV driver laser will have a maximum power of 1 W in CW operation which can be absorbed in the cathode. All together the power input to the cathode amount to 20 W. The liquid nitrogen cooling system should prevent that this power goes into the He path. Thereby the crucial point is the connection between the photocathode and the cooling system. The photocathode is fixed in a cooling unit by a bayonet socket system. A spring affords the force between the touched cone areas of the photocathode and the cooling unit. The cooling unit is connected to the liquid N2 reservoir which temperature amounts 77 K.

In a test bench the effective cooling of the photocathode was checked. In a vacuum chamber the complete cooling system together with a photocathode was installed and connected to a liquid N_2 dewar. In order to simulate the power input of rf and laser, an electrical heater was mounted on the top of the cathode. A number of temperature sensors was installed to monitor the behaviour of the cooling system. A photograph of the vacuum flange with the installed components is shown in Fig. 3.

Fig. 3: Flange of the test bench with the cathode cooling system.

The measured temperatures of the cathode in Fig. 4 (curves [1a,b,c,d]) shows an improvement of the thermal conductivity between the cathode and the cooling body. By the heat process the liquid N2 reservoir (curve [3]) retains 77 K and the cooling body (curve [2]) shows a negligibly increasing temperature. The starting temperature value (curve [1a]) of the cathode amounts $\Delta T = 64.6$ K with regard to liquid N2 temperature. An improved matching of the touched cone shapes leads to a temperature value (curve [1b]) of $\Delta T = 40.6$ K. In a next step, the spring is strengthened from roughly 20 N to roughly 39 N elastic force. The temperature (curve [1c]) decreases to $\Delta T = 28.8$ K. Once more the matching of the touched cones are improved, so the final best low temperature value of $\Delta T = 21.9$ K is achieved (curve [1d]).

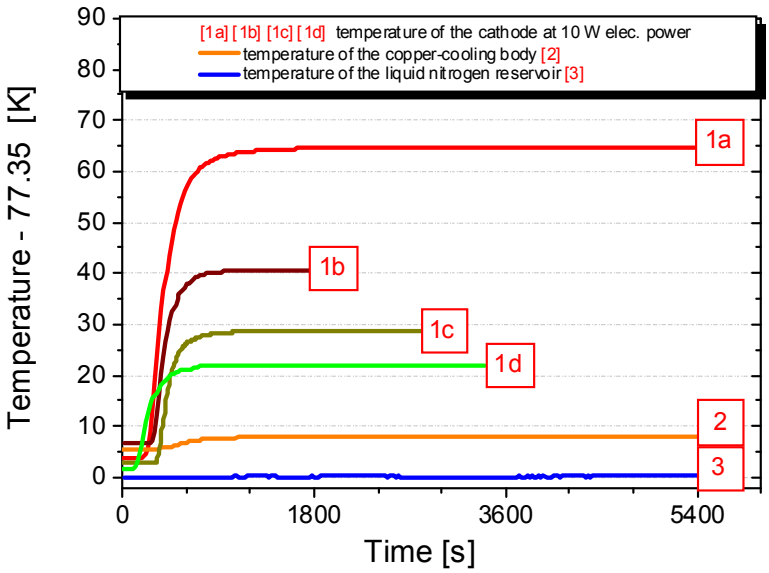

Fig. 4: Results of the test bench measurements.

This temperature corresponds to a radiation power of roughly 8.6 mW from the cathode calculated by Stefan-Boltzmann law (~ 0.2% from the cooling power of the helium system).

3. Mechanical Properties of the Cavity Tuner System

For the SRF gun cavity a frequency tuning is needed for the choke filter, the half-cell and the three TESLA cells. The bandwidth of choke filter is comparably large. Therefore a tuning during assembling in the warm stage is sufficient. For the accelerating cells tuning is required during operation. The half-cell on one hand and the three TESLA cells on the other essentially differ in their mechanical properties, especially in their stiffness. Therefore it was decided to use two separate tuning systems, one for the half-cell and one for the three TESLA cells in common.

The tuner design was adopted from the ELBE cryomodule dual spindle-lever tuning system [15]. But an essential modification of the tuner design for the SRF gun cavity was necessary due to many mechanical and cryogenic constraints and the insufficient clearance at cathode side of the cavity and the He tank. Fig. 5 shows the design of the tuning system together with the cavity. The tuner mechanism consists of a spindle with partly left-hand thread and right-hand thread and two levers. Via the threads and the lever system the rotational motion is transformed into a longitudinal motion performing the length variation of the half-cell and the TESLA cells, respectively. The use of two levers ensures that no axial force is present on the spindle. The bearing point of the leverage system has no rotational parts. It consists of two flexible links as it is shown in Fig. 6. The advantage is the lack of any hysteresis due to friction effects and bearing clearance. The third flexible link is connected with a moving bolt which transfers the force to the parts of the He tank joint to the end plates of the half-cell or the TESLA cells.

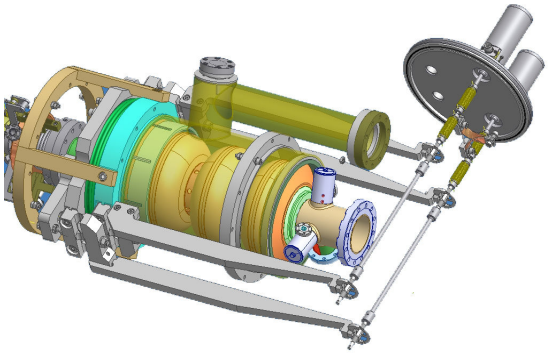

Fig. 5: The two tuners of the SRF gun.

Fig. 6: Tuner lever with flexible link.

The frequency constants Δf/dL of the SRF gun cavity were measured with the help of the warm tuning machine developed at FZR (see section). The measurement results are 254 kHz/mm for the half-cell and 449 kHz/mm for the three TESLA cells. These values belong to the change of the π mode frequency of the whole cavity, where the three TESLA cells were unchanged in the first case, and the half-cell in the second. Simple numerical estimations with SUPERFISH [12] assuming a smoothly and homogeneous change of the surface contour give 674 kHz/mm for the half-cell and 625 kHz/mm for the TESLA cell tuning. The large difference for the half-cell seems to be an effect of the low stiffness of the end disk or of other weak areas having low influence on the frequency.

For operating tests and parameter measurements a test bench for the designed tuning system was built up [16]. This test bench consists of the liquid nitrogen dewar, the leverage of the tuner, a spring packet to simulate the cavity, and the equipment to produce the tuning force, to perform force and length measurements. The spring packet, shown in Fig. 7, was variable in order to simulate the half-cell and the three TESLA cells, as well as to measure with preload. For the three TESLA cells a spring constant of 9 kN/mm was taken [17]. The spring constant for the half-cell was assumed to be about three times higher. The preloads were varied between zero and 9 kN. In comparison to the final tuning systems the levers were made of aluminium instead of titanium and the tests were carried out with one lever only. The complete mechanical arrangement mounted in the nitrogen dewar is shown in Fig. 8.

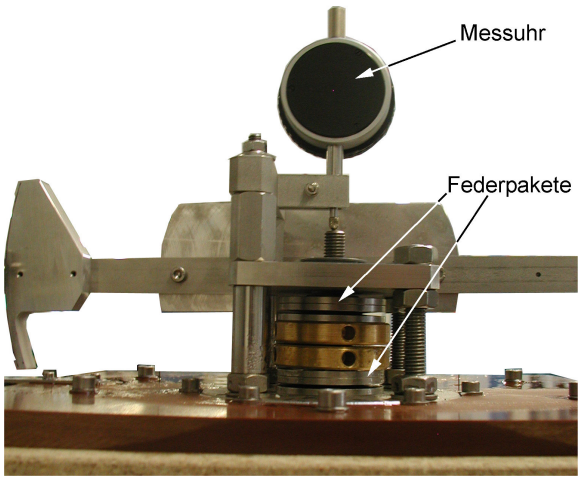

Fig. 7: The spring packet of the tuner test bench simulates the cavity.

Fig. 8: The mechanical arrangement of the test bench with the tuner lever and link to be tested.

A typical measurement diagram is presented in Fig. 9. It shows the length change at the spring packet (cavity) as a function of the lever motion for different spring constants D and pre-load forces F_v. The hysteresis in the curves is caused by the test bench, not by the tuner itself. The measurement results are summarized in Table 2. As expected, the tuning range became smaller with 5 kN preload due to the elastic behaviour of the flexible link. Fatigue effects were not found.

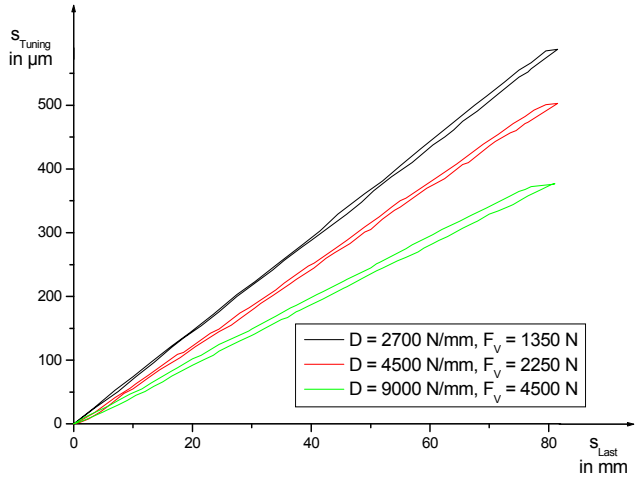

Fig. 9: Tuning length versus lever motion for three different spring constants and pre-loads.

Table 2: Measurements of the tuning ranges in the tuner test bench.

Tuning range for 2° Lever range	half-cell tuner	TESLA cell tuner
without preload D = 0 N/mm	436 µm 416 kHz	450 µm 247 kHz

with 5000 N preload D = 9000 N/mm	218 µm 208 kHz	223 µm 122 kHz

Table 3 presents the properties of the two tuners for the SRF gun including the test bench results. The limit in the tuning range is given by the maximum bending of the flexible links of ± 1.5°. The expected tuning ranges are sufficient. By comparison, the tuning range in the ELBE modules is 230 kHz [15]. The overall tuner resolution given in the table are estimations taken from the ELBE system.

Table 3: Parameters of the SRF gun tuners.

	half-cell tuner	TESLA cell tuner
lever length	630.6 mm	570.2 mm
leverage	50.4	44.2
lever range	33 mm 3.0°	30 mm 3.0°
tuning range	0.7 mm 204 kHz	0.7 mm 404 kHz
cavity frequency constants Δf/dL	178 kHz/mm	283 kHz/mm
mechanical drive step	0.70 nm/step	0.62 nm/step
frequency drive step	0.23 Hz/step	0.28 Hz/step
mechanical resolution	3 nm	
frequency resolution	1 Hz	
position of step-motors	warm, outside	

4. Cryostat

4.1 Magnetic shielding

One important aspect for superconducting accelerators is the reduction of the magnetic field flux through the cavity material during the cooling down procedure. For the Nb cavity of the SRF-Gun, a specially designed µ-metal shield was fabricated and the remained magnetic field inside the µ-metal shield had to be measured. To prevent any effect on the performance of the cavity, the remaining magnetic field should be less than about 1 µT [18]. The magnetic field of the earth amounts approximately 50 µT.

With a Hall-Probe which was guided concentric in the µ-metal shield at reproducible places the three components of the magnetic field were measured. Analogously, the magnetic field was determined inside the stainless-steel vessel which encloses the µ-metal shield.

The results of the earth magnetic field measurements with and without screening are shown in Fig. 10. The values in X Y orientation are an average of 3 measurements with a total error of +/ 0.003 G. The unshielded earth magnetic field amounts to approximately 0.5 G = 50 µT. Inside the µ-metal shield the magnetic field is reduced to approximately 0,007 G = 0.7 µT.

The screening of the steel vessel leads to a reduction of the earth magnetic field to approximately 0.4 G = 40 µT. The vessel encloses the µ-metal shield, hence the total screening value can be estimated to a magnetic field < 0,007 G = 0.7 µT. Furthermore, the measurement of the X Y direction with an approximately average of 0,002 G = 0.2 µT shows, that the main part of the magnetic field is oriented in Z direction. The results in Fig. 10 show that the µ-metal shield reduces the earth magnetic field by a factor of 70. Even in the edge area of the shield a good screening is obtained. The reduction of the earth magnetic field is relatively constant about the whole length of the µ-metal. With an average value of approximately 0.8 +/-0.5 µT, the requirement to reduce the earth magnetic down to some µT is well done. The position of the superconductive cavity inside the magnetic shield is indicated in Fig. 10. The cavity is by far shorter than the µ-metal shield Therefore the cavity is not influenced by the less well screened edge areas. Furthermore, a varying screening behaviour of the µ-metal under LN_2 temperature conditions was not observed. The measurement accuracy was +/-0.5 µT. Therefore, a possible shield failing during the cool down procedure is not expected.

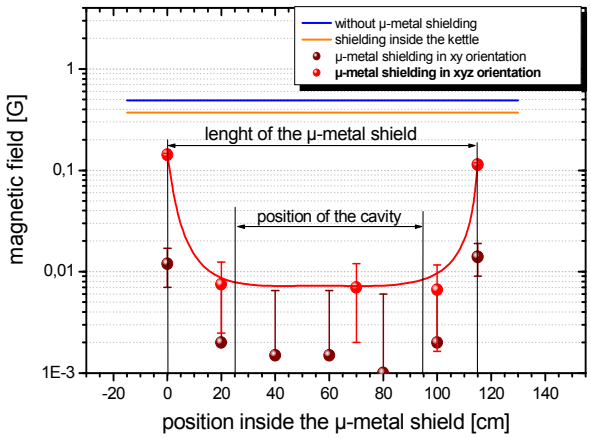

Fig. 10: Earth magnetic field with and without µ-metal screening.

4.2 Assembly and test of the SRF gun cryostat

End of 2006, the SRF gun cryostat was assembled with a dummy instead of He tank and niobium cavity. The following components were tested: vacuum vessel, thermal shield, liquid nitrogen system, cathode support and cooling system, nitrogen and helium ports, RF port and power coupler, cavity alignment and support system, cavity tuners, and temperature sensors. During this test period the vacuum vessel was pumped to $1x10^{-5}$ mbar and the cryostat was cooled down with liquid nitrogen (80 K). Leak tests of the isolation vacuum and the nitrogen system were carried out.

4.3 Test of the cathode alignment system

The cathode alignment system allows for the alignment of the photocathode in the cavity with respect the cavity axis. This can be performed from outside the cryostat by means of three rotational feed-throughs. Furthermore, the position of the cathode can be varied with respect to the backplane of the cavity half cell. This system was tested to obtain alignment accuracy

and reproducibility and to determine the range for the cathode motion. A photograph (fig. 11) shows the arrangement.

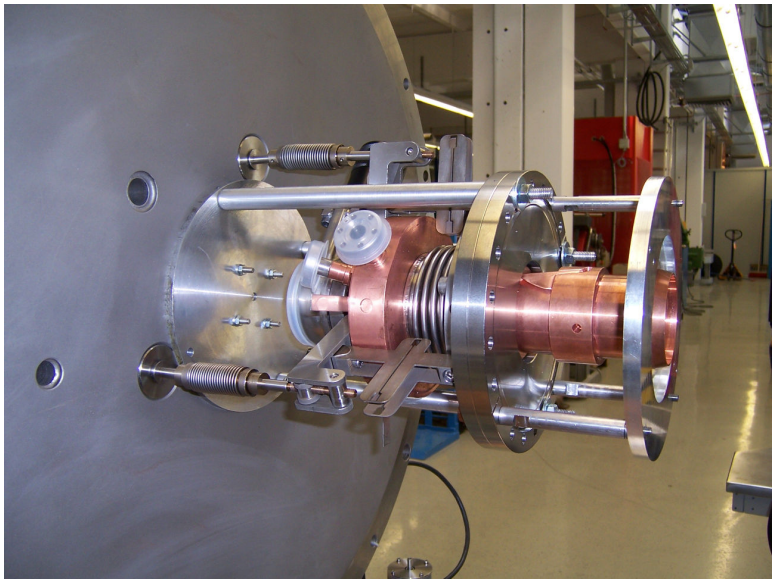

Fig. 11: Photograph of the cathode cooling unit with cathode alignment system.

5. Niobium Cavity

5.1. Field profile and warm tuning

In order to get the right field distribution and the accurate frequency at operation inside the cryostat, one has to consider different tuning parameters. The correct frequency at room temperature mainly depends on cool down shrinking, additional chemical treatment and pre-stressing of both cavity tuners. These tuners permit an axial deformation of ±400µm and ±500µm for the half cell and the three TESLA cells, respectively. The induced frequency shifts have been taken into account. Thus, the estimated tuning frequency follows from Table 4.

Table 4: evaluation of the estimated frequency @ 300K

operating frequency @ 2K	1300.0 MHz
cool down shrinking (measured @ ELBE)	- 1.97 MHz
50µm BCP @ DESY (simulated)	+ 0.55 MHz
pre-stressing half cell (measured)	+ 0.10 MHz
pre-stressing three TESLA cells (measured)	+ 0.22 MHz
required frequency @ 300K	1298.9 MHz

The electric field distribution on the cavity axis is measured by a fully computer controlled bead pull measuring device that is based on the diploma thesis of Peschke [19]. Due to the prestressing of the cavity cells in the cryostat, the detuning of the π-mode field has to be considered inversely during the warm tuning to obtain the "flat" field profile in the cryostat. Table 5 shows the non-negligible the measured variation from the optimum.

Table 5: field detuning caused by pre-stressing of the cavity cell

	Gun Cell	TESLA1	TESLA2	*End Cell*
detuning axis field	**-7.3%**	**-1.8%**	**+1.4%**	**+3.1%**

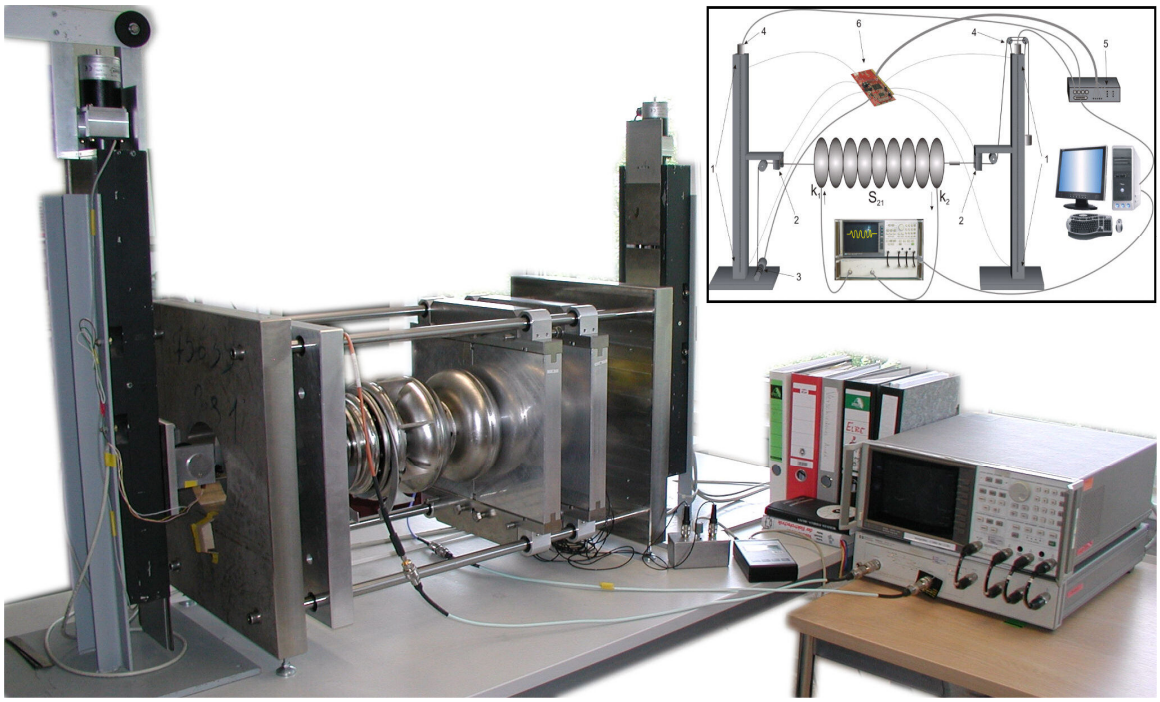

Fig. 12: tuning device with integrated bead pull measurement

Based on these target values, the tuning process was realized by the single iteration tuning method as proposed by Cooper [20]. Since the gun cell and the choke filter are different in shape from the TESLA cells the existing tuning machines for TESLA cavities cannot be used for the SRF gun cavity. Rather a modified tuning machine had to be built which is shown in Fig. A1. By this device all cells were manually pushed or pulled to the calculated frequencies. In order to get the same electric peak surface fields for the π-mode in all four cells, the on axis peak field Ez in the gun cell has to be 60% of the peak field in the TESLA cells.
The resulting field profiles before and after tuning are shown in Fig. 13. The adjusted field distribution perfectly met the calculated requirements. The corresponding pass band frequencies are presented in Fig. 14.

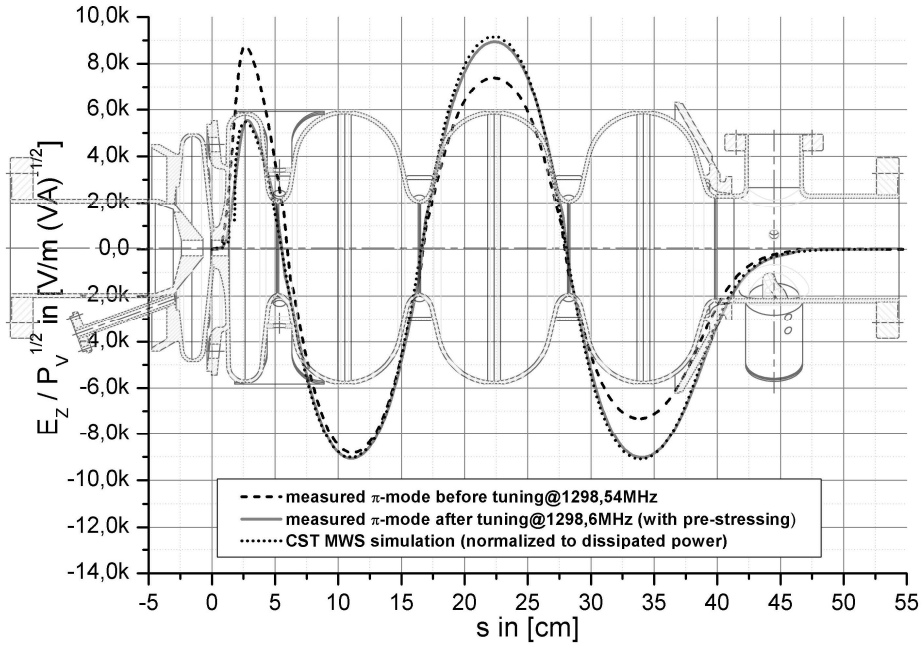

Fig. 13: measured vs. simulated π-mode field profiles before and after tuning.

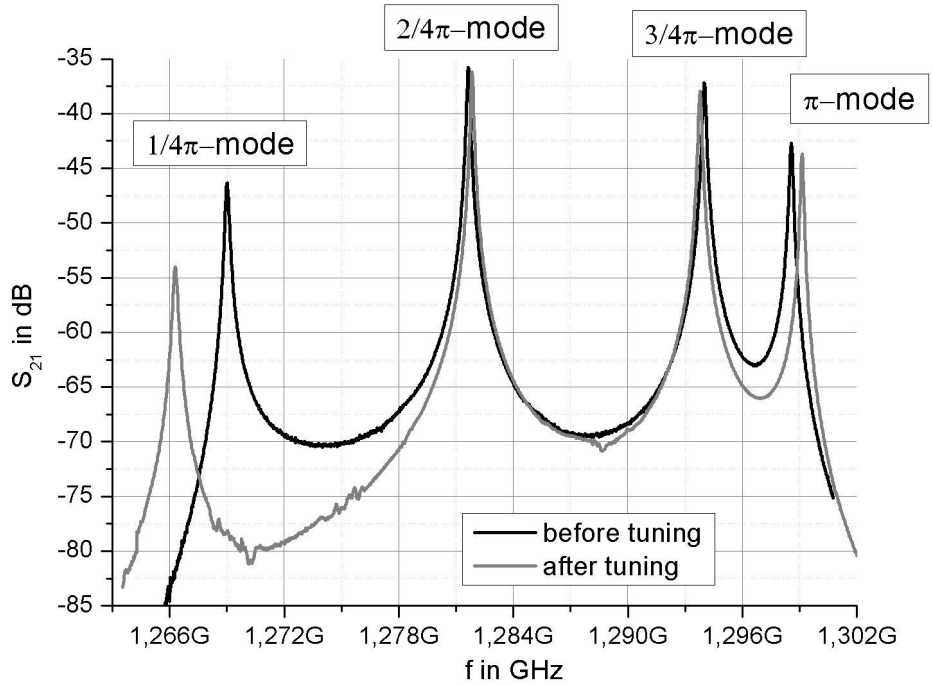

Fig. 14: Pass band frequencies before and after warm tuning.

5.2 Ext. Q study main-Coupler

In order to optimize the rf power transfer from klystron to the electron beam, it is necessary to match the coupling. The applied Rossendorf main coupler is not adjustable, thus the antenna is optimized for a bandwidth of 100Hz and an external quality factor of:

$$Q_{ext} \approx Q_L = \frac{f_0}{B} = \frac{1.3GHz}{100Hz} = 1.3x10^7 \quad (1)$$

The determination of the suitable distance between antenna tip and axis of rotation is done by an additional probe antenna added at the opposite side of the cavity at room temperature. As shown in equation 2 one has to measure incident and reflected power at the input port, the transmitted power at the main coupler as well as the unloaded quality factor of the cavity.

$$Q_{ext} = \frac{Q_0}{\beta_{ext}} \quad with \quad \beta_{ext} = \frac{P_t}{P_i - P_r - P_t} \tag{2}$$

The results presented in Fig. 15, point to the required coupling at a distance of 43.2 mm from axis. An additional calculation, using the results of MWS©-simulations with different boundary conditions as shown in [21], gives a similar performance.

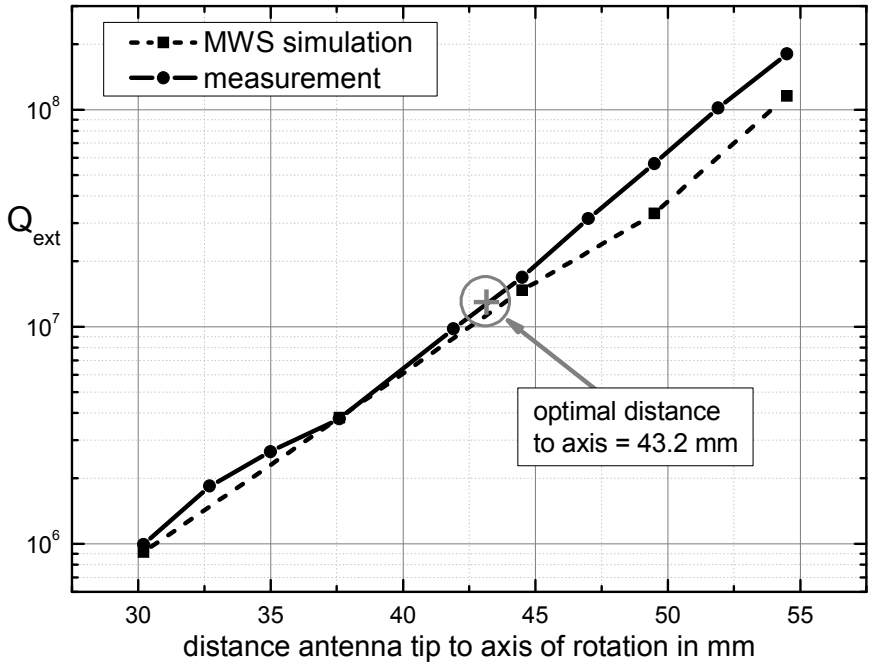

Fig.15: external quality factor vs. antenna length.

5.3 Tuning Chokefilter

The filter is designed as a coaxial trap filter. We measured the external quality factor versus detuning of the choke cavity by crushing and stretching. For this purpose an antenna probe with the same diameter as the original cathode was used. Thus the power behind the choke filter depending on the dissipated power through the walls can be measured (Fig. 17).
As a result one gets a tuning curve shown in Fig. 16. Due to mechanical tolerances during the assembling of the cryostat, it is hard to improve the accuracy better than ±100 microns. Within this range, the external quality factor is better than Qext=10^{12} and the power leakage is less than 1% of the dissipated power.

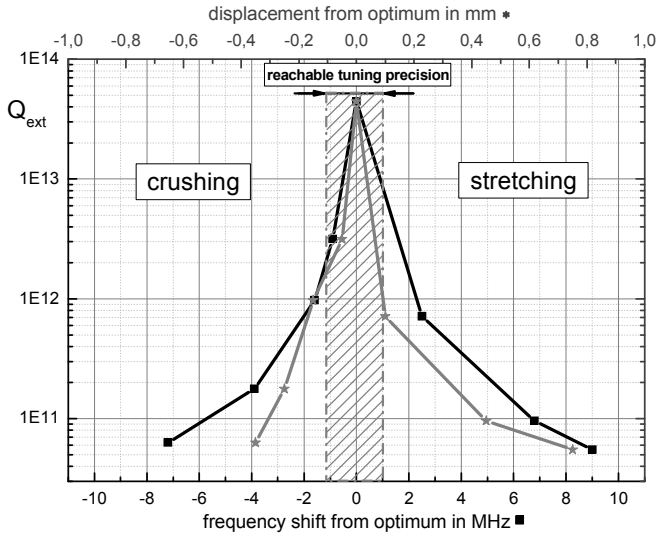

Fig.16: external quality factor vs. choke filter detuning measured by frequency shift and deformation.

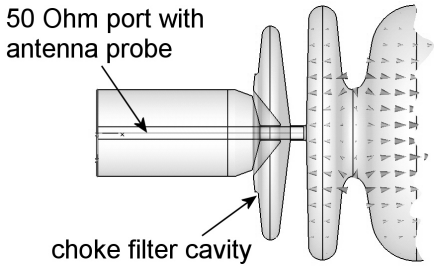

Fig. 17: assembly to measure π-mode suppression.

5.4 Tuning HOM-Coupler

To estimate the precision achieved by the trap circuit tuning, we measured the external quality factor at the π-mode frequency versus tuning displacement and frequency shift. To prevent crosstalk it is necessary to place the input antenna probe at the opposite side of the HOM couplers. The result is presented in Fig. 18.

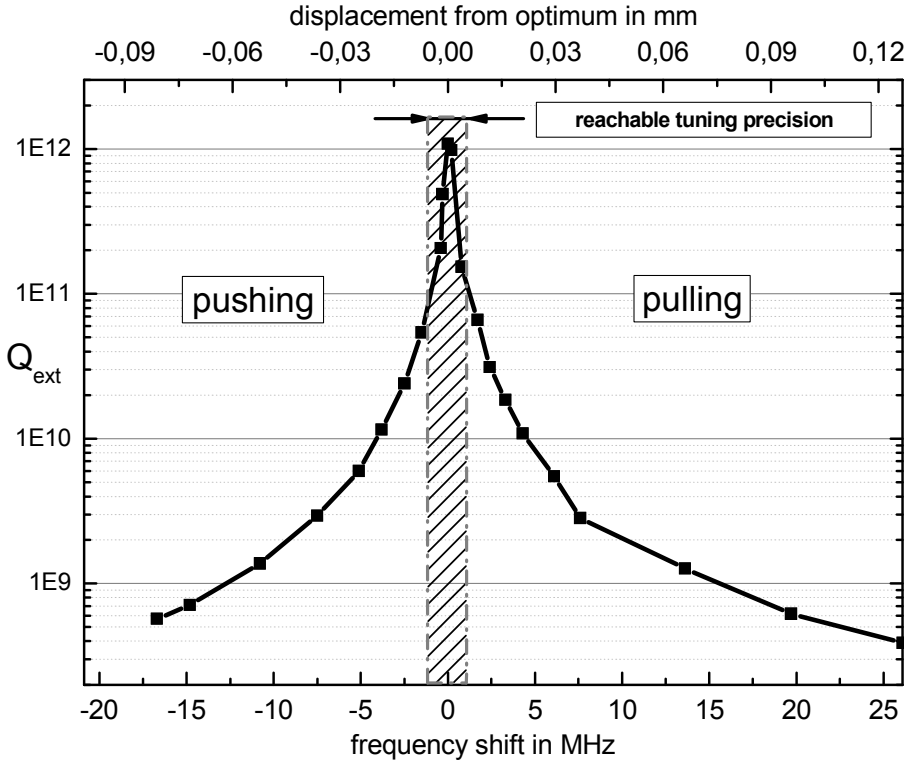

Fig. 18: external quality factor vs. detuning from best π-mode suppression.

It is obviously hard to get a better external quality factor than Qext=10^{11}. In that case less than 10% of the dissipated fundamental power is transmitted out of each HOM-coupler.

5.5. Measurements in the vertical test bench

5.5.1 1st vertical cold test

Following the tuning procedures the cavity was prepared at DESY Hamburg by buffered chemical polishing (40µm BCP) and high pressure rinsing (HPR). Afterwards the cavity was tested in a vertical cold test, as described in [22]. During the cool down from 4.4 K to 1.6 K the unloaded quality factor was measured at low rf power (Fig. 19). The illustrated surface resistance follows from eq. 3 and the numerical calculated geometry factor G.

$$R_S = \frac{G}{Q_0} \quad with \quad G = 241.9\Omega \tag{3}$$

Based on the BCS-theory the surface resistance can also be calculated analytically. Fitting the measured data points by using eq. 4 leads to the following material parameters:

$$A_S = 2.42 \cdot 10^{-15} \frac{\Omega \cdot K}{Hz^2} \quad ; \quad \Delta = 1.53 meV \quad ; \quad \underline{R_{res} = 3.43 n\Omega}$$

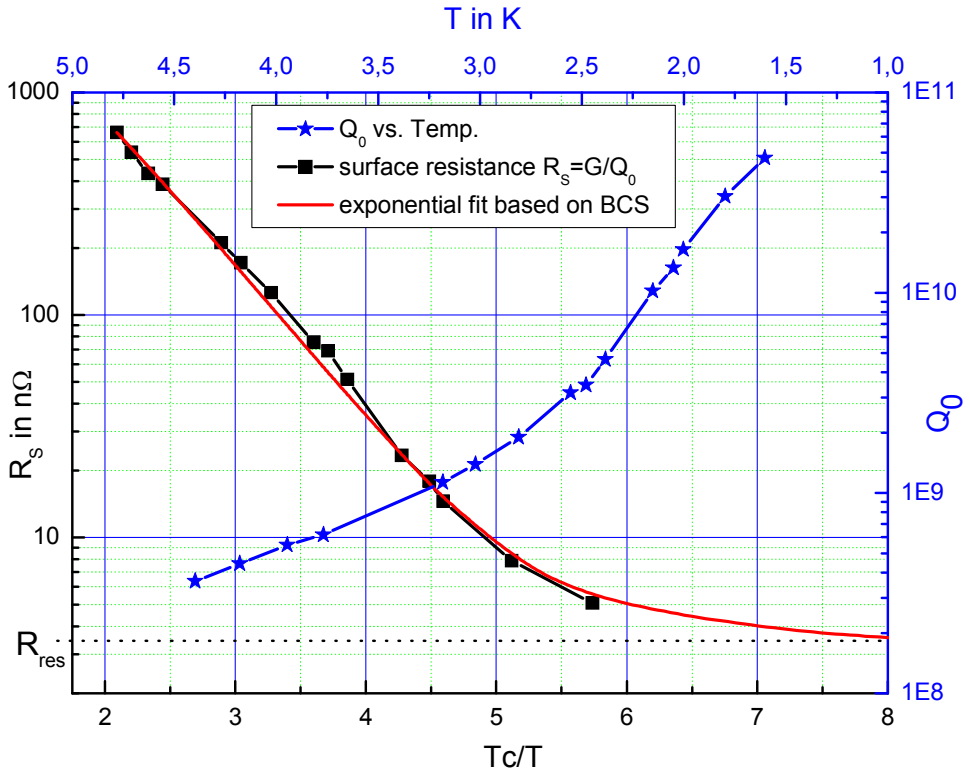

Fig. 19: surface resistance and unloaded quality factor versus temperature.

$$R_S = A_S \cdot \omega^2 \cdot \frac{1}{T} e^{-\frac{\Delta}{k \cdot T}} + R_{res} \quad \text{für} \quad T < T_C / 2 \tag{4}$$

In view of the measured, unloaded high quality factor of Q_0(@1.8K)=3x10^{10} and the calculated low residual resistance of R_{res}=3.4nΩ the preparation of the cavity proceeded well. Another matter of substantial interest is the Q vs. E chart. In order to get comparable values, Q_0 is plotted versus peak axis field in the TESLA cells (design value E_{peak}=50MV/m).

Furthermore the radiation caused by field emitters is included into the same chart. As shown in Fig. 20, field emission started early and the quality factor decreases. Further increasing of rf power results in strong field emission and two Q-switches, which are probably caused by thermal breakdown at activated field emitters. After the second Q-switch the field was limited by quench. Especially the behaviour of the Q-switches is most likely due to defects in the bulk niobium or to surface pollution. This might be induced by the hardly cleanable choke filter. Because of the narrow cathode feed through between choke filter and gun cell, direct cleaning of the filter cell wasn't feasible. Furthermore contaminated water runs out of it into the cavity which leads into polluted surface.

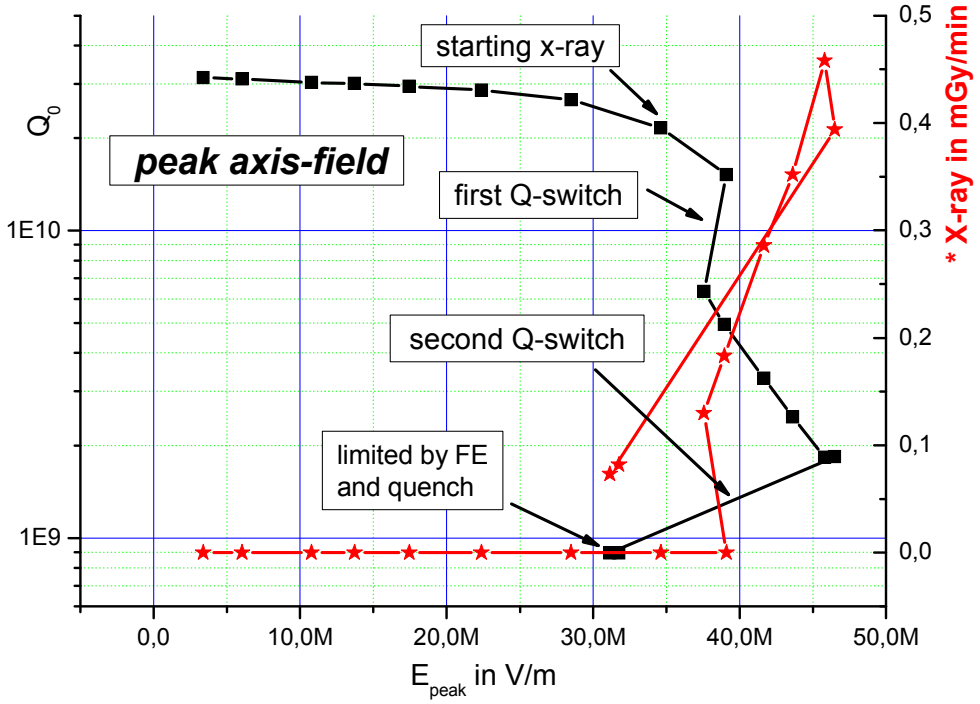

Fig. 20: Q_0 and radiation vs. peak axis field E_{peak} @1.8K (1st vertical test bench)

5.5.2 4th vertical cold test

Based on the experience of the first vertical test bench, an improved cleaning was realized by the company ACCEL Instruments GmbH. A special high pressure rinsing lance was built to enable an additional cleaning of the choke filter beside the established preparation of the cavity cells. Due to technical problems during the cleaning the achieved results of the followed 2nd and 3rd tests are negligible (fig 21).
Caused by the shortage of time the 4th preparation and the vertical test bench had to be the base for further assembly. As shown in fig. A11 the first measurement started very promising. But unfortunately a Q-switch at 27 MV/m paired with the beginning of field emission decreased the quality factor and the maximum electric peak field. The last measurement of the π-mode after several tests resulted in the red Q_0 vs. E_{peak} curve. In comparison to the first curve we found no Q-switch but the field emission started much earlier und thus the quality factor decreased. This performance is probably caused by a field emitter that was activated during the first measurement at the Q-switch. This assumption is supported by a small scratch that we found inside the cavity at the back plane of the half cell. The damage results from a collision between the cavity and the high pressure rinsing lance during the cleaning. We are confident that the field emission was caused by the scratch. So its removal will result in a

better performance. Unfortunately there is no time for a 5th vertical test bench so we have to wait for further tests until the cryostat is completely assembled.

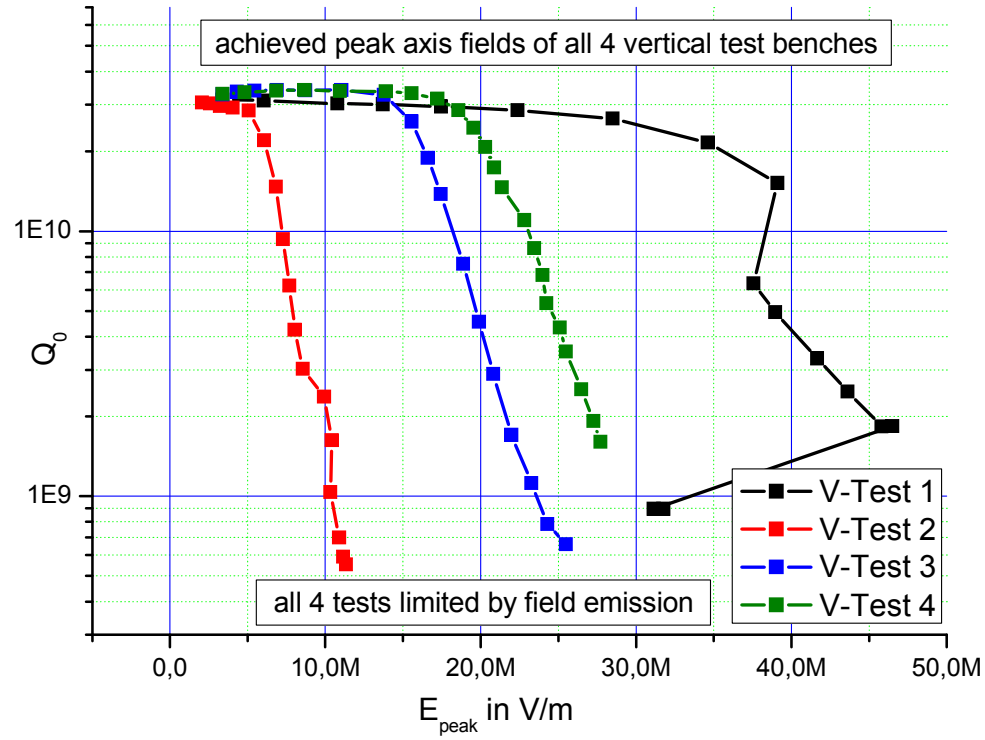

Fig. A21: comparison between the achieved E_{peak} for the π–mode in all tests

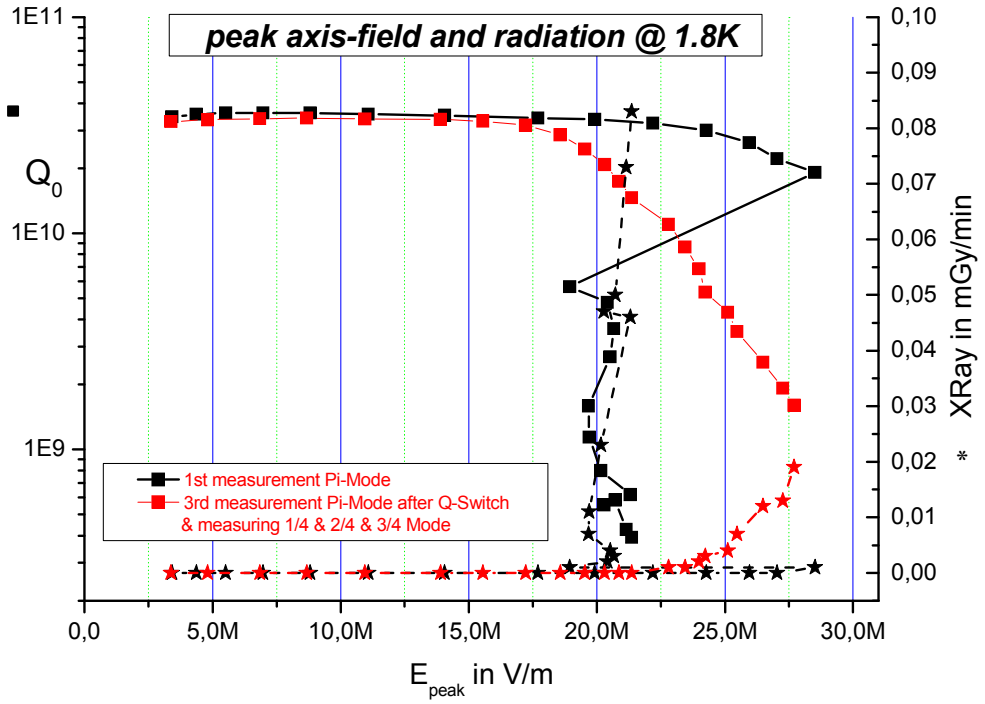

Fig. A22: Q_0 and radiation vs. peak axis field E_{peak} @1.8K (4th vertical test bench)

Even though the cavity performance keeps at a level of about 50% of the designed values, it will be possible to demonstrate the advantages and to collect important experiences in operation of such electron sources.

Acknowledgements

We acknowledge the support of the European Community-Research Infrastructure Activity under the FP6 "Structuring the European Research Area" programme (CARE, contract number RII3-CT-2003-506395)

References

1. D. Janssen, et al., "Status of the 3 ½ cell Rossendorf superconducting RF gun" Proceedings of 2004 FEL Conference, 359-362
2. J. Teichert, et al., "A superconducting photo-injector with a 3 ½ cell cavity for the ELBE LINAC", Proceedings of EPAC 2004, Lucerne, Switzerland
3. J. Teichert, et al., "Overview of the present status of the SRF gun design and construction", CARE Note-2004-010-ELAN
4. R. Xiang, et al., „Status of 3½ cell superconducting rf gun project in Rossendorf", Proceedings PAC 2005
5. F. Staufenbiel, et al., „Test of the photocathode cooling system of the 31/2 cell SRF gun", Physica C 441 (2006) 216-219
6. C.D. Beard, J.H.P. Rogers, F. Staufenbiel, J. Teichert, "3-1/2 Cell Superconducting RF Gun Simulations", EPAC 2006, Edinburgh, Scotland, June 26 – 30, 2006
7. D. Janssen, et al., "Progress of the Rossendorf SRF Gun Project", EPAC 2006, Edinburgh, Scotland, June 26 – 30, 2006
8. I. Will, G. Klemz, F. Staufenbiel, J. Teichert, "Photocathode Laser for the Superconducting Photo Injector at the Forschungszentrum Rossendorf", FEL 2006, Berlin, Germany, Aug. 27 – Sept. 01, 2006
9. J. Teichert, et al., "Cryomodule and Tuning System of the Superconducting RF Photo-Injector", FEL 2006, Berlin, Germany, Aug. 27 – Sept. 01, 2006
10. A. Arnold, et al., "First RF-Measurements at the 3.5-Cell SRF-Photo-Gun Cavity in Rossendorf", FEL 2006, Berlin, Germany, Aug. 27 – Sept. 01, 2006
11. A. Arnold, et al., "The Rossendorf SRF Gun Project", Nuclear Instruments and Methods in Physics Research A, submitted
12. J.H. Billen and L.M. Young, "POISSON SUPERFISH", LANL, LA-UR-96-1834, revised April 2000.
13. P. vom Stein, „Hochfrequenz Elektroneninjektoren für cw-Beschleuniger", PhD thesis, Dresden University of Technology , 1998, Report FZR-227
14. A. Michalke, "Photocathodes inside a Super-conducting Cavity", PhD thesis, University of Wuppertal, 1993, WUB-DIS 92-5
15. J. Teichert, et al., "RF Status of Superconducting Module Development Suitable for CW Operation: ELBE Cryostats", Nucl. Instr. and Meth. A 557 (2006) 239.
16. René Hempel, "Messung der mechanischen Eigenschaften eines Tuners für einen supraleitenden HF-Resonator", diploma thesis, HTW Dresden, 2005
17. C. Pagani et al., "Improvement of the Blade Tuner Design for Superconducting RF Cavities", Proc. of PAC 2005, Knoxville, USA, p. 3456.
18. B. Aune, et al., Phys. Rev. Special Topics, Vol. 3 (2000) 092001
19. Peschke, Claudius: „Messung und Berechnungen zu longitudinalen und transversalen Shuntimpedanzen einer Elektronen-Positronen Linearbeschleuniger-Struktur", Frankfurt a. M., J.W.Goethe-Universität, Dipl.-Arb., 1995
20. C. Cooper, "Single Iteration Tuning for Multicell RF Cavities for Cornell ERL". In: REU research reports (Aug. 2003), Cornell University, NY
21. P. Balleyguier, "External Q studies for APTT SC-Cavity Couplers", CEA/DPTA, Bruyères-le-Châtel, France.

22. J. Knobloch, “Basic Concepts of Measurements Made on Superconducting RF Cavities”, Laboratory of Nuclear Studies, Cornell University, August 1991.